

RESEARCH

Open Access



# Freeze–Thaw Resistance of Ternary Blended Concrete Using Ferronickel Slag

Won Jung Cho<sup>1\*</sup>  and Min Jae Kim<sup>2</sup>

## Abstract

The present study investigated the resistance of concrete blended with ground granulated blast furnace slag (GGBS) and ferronickel slag (FNS) to cycles of freeze and thaw. The replacement ratio of the binders was 0%, 50 wt% of GGBS and 30 wt% of GGBS + 20 wt% of FNS for O100, OG50 and OG30F20, respectively. Specimens consisted of cement paste and concrete kept at 0.45 water/binder ratio. After 28 days of curing, specimens were subjected to freeze and thaw cycles (300) for measuring the variation of strength, weight loss and fundamental transverse frequency. Simultaneously mercury intrusion porosimetry was performed to examine the pore structure modifications at 28 days. The hydration products for cement paste cured at each determined age were characterized by X-ray diffraction and the content of CH and CSH was obtained from thermogravimetric analysis (TGA). As a result, the ternary blended concrete specimens showed lower deterioration degree when subjected to the freeze and thaw cycles. This may be due to a latent hydraulic and/or pozzolanic reaction producing more CSH in the matrix, which in turn increases the volume of small pores. The increased content of C–S–H gel for OG30F20 was confirmed by TGA, accounting for 69.9%. However, the binder system consisting of ordinary Portland cement and GGBS did not exhibit higher resistance to the given deleterious environment, presumably due to a delayed hydration process.

**Keywords:** ferronickel slag, blast furnace slag, freeze–thaw, mineral admixtures, ternary blended

## 1 Introduction

Concrete is an indispensable construction material. Its utility has been yearly increasing at the rate of 6% (Ghods et al. 2017) and demand is also rising. Although it is necessary material for a construction structure, constantly considered one of the most energy-intensive industry (Rahman et al. 2017; Lemonis et al. 2015). Besides, about 5% of the carbon dioxide produced is due to cement production and worldwide, roughly 900 kg CO<sub>2</sub> is produced per ton of cement (Rahman et al. 2017; Lemonis et al. 2015; Neville 1995; Mahasanen et al. 2003). Furthermore, this is not possible to be sure that the two issues mentioned above were calculated on a like-for-like base (Winter 2012). In line with this situation, global environmental

load reduction policies, such as carbon emission rights, clean development mechanism were enforced. Nevertheless, it is estimated that 5.8 billion tons of cement will be produced by 2050 (Scrivener 2012). Therefore, the focus of research on supplementary cementitious materials (SCMs) needs to be conducted more to correspond this production.

Ground granulated blast furnace slag (GGBS) which is a by-product in the manufacture of pig iron in the blast furnace has been used successfully as SCMs since the discovery of the latent hydraulic reactivity at the end of the nineteenth century (Matthes et al. 2018). This GGBS provides advantages to concrete, lower permeability, higher sulfate and acid resistance, long-term strength and lower heat of hydration (Öneret et al. 2003). However, this traditional admixture cannot be easily obtained in many places (Huang et al. 2017). For the case of South Korea, the recycling rate of GGBS is close to 100% due to the surge in use (Koh and Ryu 2011). Thus the dependence on imports is increased, but it has not been resolved because

\*Correspondence: nelly91@hanyang.ac.kr

<sup>1</sup> Department of Civil and Environmental Engineering, Hanyang University, Ansan 15588, Republic of Korea

Full list of author information is available at the end of the article  
Journal information: ISSN1976-0485 / eISSN 2234-1315

of inequality in supply and demand. Moreover, there is a shift to embrace other materials, which is driven by many factors, including supply-and-demand concerns (Juenger and Siddique 2015). Accordingly, finding new SCMs is exigent issue not only for replacement of cement, but also complementation of conventional mineral admixtures.

Ferronickel slag (FNS) is a by-product from primary industry of smelting of laterite ore in an electric arc furnace at a high temperature in the presence of a reducing agent, for the production of ferronickel. It is assumed that 1 ton of ferronickel may generate about 14 tons of FNS. In Korea, approximately 2 million tons of FNS are produced (Cho et al. 2018) and 30 million tons are discharged in China annually (Pang et al. 2015). This large amount of FNS is being landfilled because of uncertainty in quality and causes soil pollution. To overcome these problems, many studies are going on for using FNS as construction materials.

FNS mainly consisted of  $\text{SiO}_2$ ,  $\text{MgO}$  and composed of crystalline minerals such as enstatite, forsterite and diopside (Choi and Choi 2015). Because of its low absorption rate, dense structure and high hardness, FNS is considered to be usable as a fine aggregate for concrete (Sakoi et al. 2013; JSCE 1994). Recently, both study about improving the strength properties of concrete (JSCE 1994; Saha and Sarker 2017) and alkali silica reactivity due to the high content of amorphous silica in FNS (Choi and Choi 2015; Saha and Sarker 2016) has been studied. Also, durability characteristics of mortar (Saha and Sarker 2018a) and concrete (Saha and Sarker 2018b) incorporating slag aggregate with traditional SCMs examined. Furthermore, research as a binder has also been actively conducted. Huang et al. (2017) suggested that replacing of cement with FNS increases the degree of polymerization of silica chains in C–S–H gel and improves the resistance of the concrete to chloride ion penetration. Potential of mineral admixture for concrete and pozzolanic activity of FNS is also observed in some studies (Lemonis et al. 2015; Katsiotis et al. 2015). Lately, in order to utilize ferronickel slag as a substitute material for cement, micro-hydration heat, flow, compressive strength and drying shrinkage variation were investigated (Cho et al. 2018). However, most of previous studies have focused on fundamental properties of FNS as a sand and SCMs reactivity. There is not enough information about the influence of FNS-blended concrete subjected to resistance of freeze–thaw environment.

Therefore, this study aims to evaluate the freeze–thaw resistance of concrete utilized with FNS as a binder. Two control specimens and ternary blended concrete containing 30% GGBS and 20% FNS were tested. In order to observe hydration reactivity, XRD, TG/DTG, MIP and SEM analysis on cement paste were conducted. Strength

development and freeze–thaw resistance such as relative dynamic modulus of elasticity, mass change, durability factor and compressive strength after freeze thaw cycles of concrete were performed.

## 2 Experimental Works

### 2.1 Raw Materials

To evaluate the durability of ternary blended concrete in terms of resistance to freeze–thaw, three types of the binder, including OPC, GGBS and FNS, were used in this study. FNS produced by a local nickel industry company in South Korea as cementitious material had  $3400 \text{ cm}^2/\text{g}$  of a specific surface area, which was determined using air permeability apparatus according to KS L 5106 (2009). The specific gravity of OPC, GGBS and FNS accounted for 3.10, 3.05 and 2.86, respectively. Chemical and physical properties of the binders are given in Fig. 1 and Table 1, respectively.

Crushed stones passed through a 20-mm sieve were used as coarse aggregate, and natural river sand was for the fine aggregate. The physical properties of the aggregates are given in Table 2.

### 2.2 Specimens Fabrications

Three types of mix proportion for paste and concrete were used in this study in order to perform the testing method including X-ray diffraction (XRD), thermogravimetric analysis (TGA), compressive strength, mercury intrusion porosimetry (MIP), relative dynamic modulus elasticity (RDME) and weight loss as shown in Table 3.

The specimens were named as O100 (100 wt% of OPC), OG100 (50 wt% of OPC + 50 wt% of GGBS) and OG30F20 (50 wt% of OPC + 30 wt% of GGBS + 20 wt% of FNS). The paste specimens were kept at 0.45 of a total W/B with no chemical admixture to avoid any adverse effect. After mixing of the dry powder with distilled water for 5 min, the pastes were placed into a cubic mold ( $50 \times 50 \times 10 \text{ mm}$ ), which was in turn cured at room conditions ( $20 \pm 2 \text{ }^\circ\text{C}$ , RH  $65 \pm 5\%$ ) for the 24 h. Then, the specimens were demolded and stored in a water bath ( $20 \pm 2 \text{ }^\circ\text{C}$ ) for specified ages. For investigating the fundamental properties and resistance to freeze–thaw, concrete specimens were fabricated into cylindrical and prism mold with an identical replacement ratio of binder and curing regime to paste manufacturing, of which the dimensions of the mold were  $\text{Ø}100 \times 200 \text{ mm}$  and  $100 \times 100 \times 400 \text{ mm}$ , respectively. Also, an air entraining agent was added to keep the air content (6%) in the cement matrix at all the mixtures.

### 2.3 Test Methods

For identifying the hydrates in the cement paste cured at 28 days, it was crushed the specimen into a piece, which

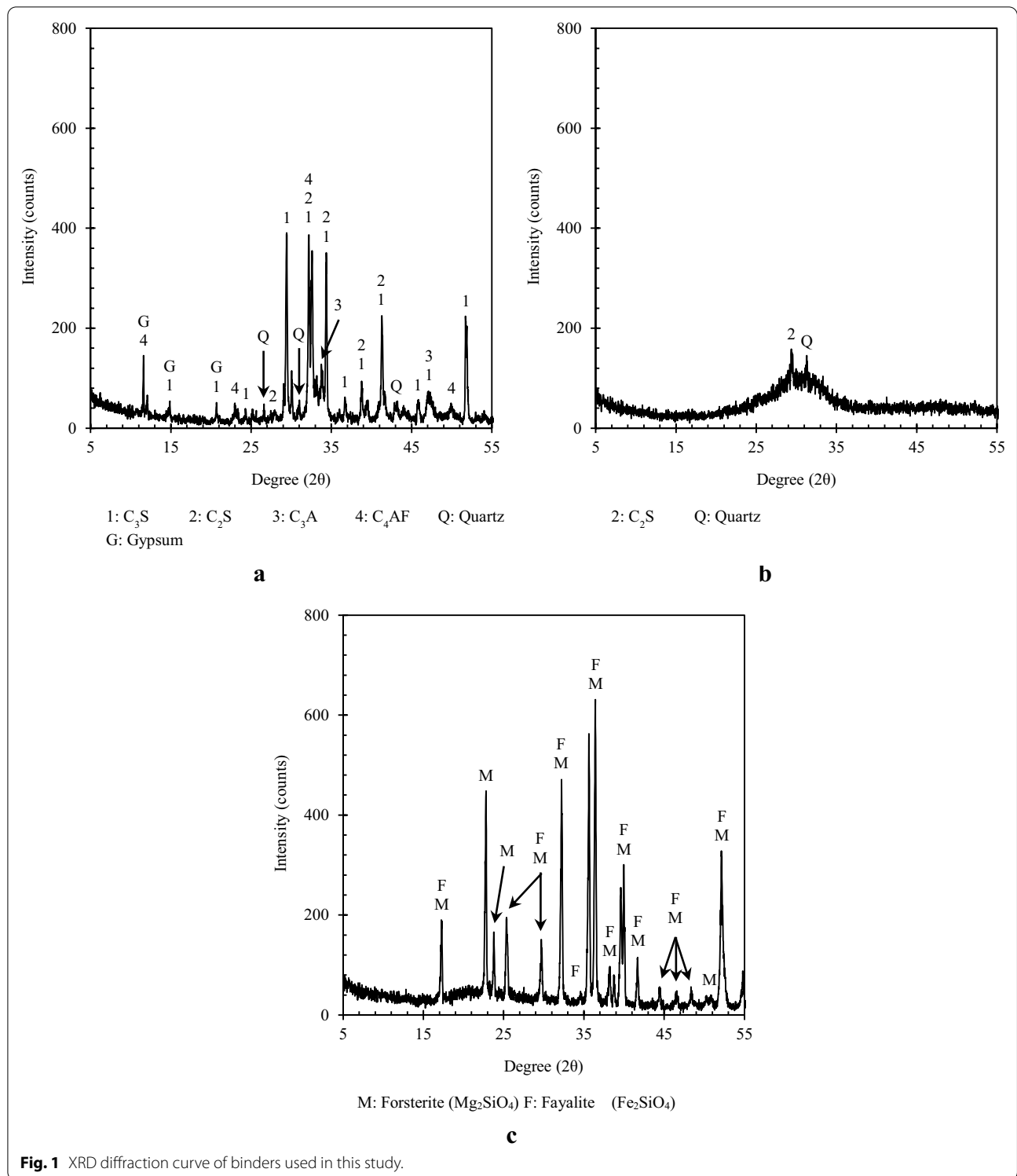


**Fig. 1** XRD diffraction curve of binders used in this study.

in turn were immersed in alcohol-based solvent for 7 days and then stored vacuum desiccator to remove the residual water in/on the sample. After that, the sample was ground and sieved with a 150-μm sieve. This powder

sample was also used in the TGA test. The XRD was conducted as using the RINT D/max 2500 (Rigaku, Japan) X-ray diffractometer, of which the test conditions were adopted as CuKα radiation with 1.5405 Å of a wavelength

**Table 1 Chemical and physical characteristics of binders (%).**

	Compounds						Loss on ignition	Specific gravity	Specific surface area (cm <sup>2</sup> /g)
	SiO <sub>2</sub>	Al <sub>2</sub> O <sub>3</sub>	Fe <sub>2</sub> O <sub>3</sub>	CaO	MgO	SO <sub>3</sub>			
OPC	17.43	3.97	4.16	66.98	1.60	3.41	1.0–1.5	3.10	3920
GGBS	28.17	12.02	0.74	50.41	2.41	4.16	1.0	2.86	4200
FNS	50.47	2.70	15.86	2.27	25.81	0.17	–0.7	3.05	3400

**Table 2 Physical properties of aggregates.**

Type	Classification	Density (g/cm <sup>3</sup> )	FM	Absorption (%)
Fine aggregate	Natural river sand	2.55	2.70	2.0
Coarse aggregate	Crushed stone	2.60	6.44	1.25

**Table 3 Mix proportions for experimental works (kg/m<sup>3</sup>).**

Abbrev.	Weight ratio						Air content (%)	Experiments
	OPC	GGBS	FNS	Water	Sand	Gravel		
Paste								
O100	1294.4	–	–	0.45	–	–	–	SEM
OG50	636.5	636.5	–					XRD
OG30F20	640.8	320.4	320.4					
Concrete								
O100	360.7			0.45	919.7	937.8	6.0	Compressive strength
OG50	179.5	179.5			915.4	933.5		RDME
OG30F20	179.8	89.9	89.9		917.2	935.1		Weight loss

at 40 kV of a voltage and 100 mA of current. In addition, due to the difficulty of detecting non-crystalline hydrates such as C–S–H gel, a TGA test was conducted using SDT Q600 (TA Instrument) to determine the composition of hydration products and their occupation at a given condition. Approximately 10–11 mg of the powder sample obtained from XRD test was placed in a crucible covered with aluminum lids, and then the temperature was increased up to 1000 °C at a 10 °C/min heating rate under a nitrogen atmosphere.

To investigate the development of strength for 180 days of curing, compressive strength for concrete made with cylindrical mold was measured using a universal testing machine with 3000 kN capacity at 140 kN/min. of a loading rate. The test was carried out on five specimens for each mix design, and the average values were used. After completing the testing of strength, it was obtained a fragment of concrete, followed by carried out an identical procedure of hydration halting to XRD and TGA test. The collected samples were initially evacuated to about 50 μm mercury, and the low pressure was generated up to 0.20 MPa by nitrogen gas. The specimen was

subsequently subjected to mercury filling pressure ranging from  $3.7 \times 10^{-3}$  to 413 MPa, so that the mercury intrusion volume was recorded at a corresponding pressure. The pore diameter was derived from the pressure using the Washburn equation as given in Eq. (1):

$$d = \frac{-4\gamma \cos \theta}{P}, \tag{1}$$

where  $d$  is the pore diameter (μm),  $\gamma$  is the surface tension (dynes/cm),  $P$  is the pressure (MPa), and  $\theta$  is the contact angle (°) which in the present study is 130°.

The resistance of the blended concrete to freezing and thawing was evaluated by measuring compressive strength, fundamental transverse frequency and weight of the specimens cured at 28 days, after exposure to cyclic environments. According to ASTM C 666—Procedure A, the temperature variation in the chamber ranged from 4 to –18 °C. For the freezing period, temperature of chamber was kept at –18 °C for 1.5 h and then increased back to 5 °C within 5.0 h. Freezing and thawing rates were kept at 10 °C/h and

repeated up to 300 cycles. Average value obtained from five specimens for each mix was used and the measurements were conducted at every 30 cycles until the assessment is possible. Consequently, the variations of compressive strength, RDME and weight loss were calculated by the following equations:

$$P_c = \left( \frac{n_c^2}{n_0^2} \right) \times 100, \tag{2}$$

where  $P_c$  is the relative dynamic modulus of elasticity after  $c$  cycles of freezing and thawing (%),  $n_c$  is the fundamental transverse frequency after  $c$  cycles of freezing and thawing (Hz), and  $n_0$  is the fundamental transverse frequency at 0 cycles of freezing and thawing (Hz).

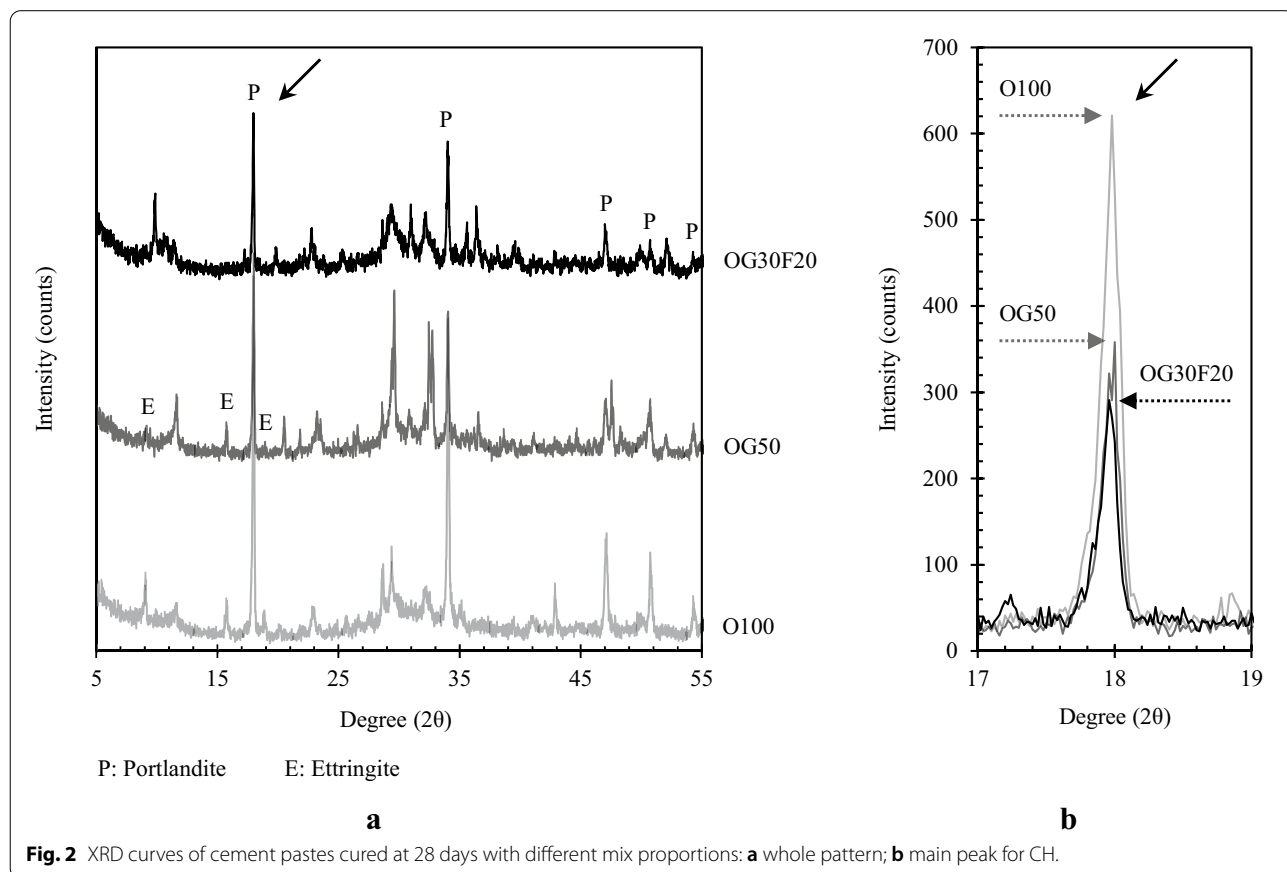
$$WL_c = \left( 1 - \frac{W_c}{W_0} \right) \times 100, \tag{3}$$

where  $WL_c$  is the weight loss after  $c$  cycles of freezing and thawing (%),  $W_c$  is the weight after  $c$  cycles of freezing and thawing (kg), and  $W_0$  is the weight at 0 cycles of freezing and thawing (kg).

### 3 Results and Discussion

#### 3.1 Hydration Products for Cement Paste Containing GGBS and FNS as Binder

An XRD test was performed to investigate the hydration products for cement paste replaced with GGBS and FNS at a given age. Figure 2a shows the XRD patterns of the blended specimens cured at 28 days. It can be seen that the main hydration products in all pastes as the crystalline form are calcium hydroxide ( $\text{Ca}(\text{OH})_2$ ; CH) and ettringite ( $3\text{CaO} \cdot \text{Al}_2\text{O}_3 \cdot 3\text{CaSO}_4 \cdot 32\text{H}_2\text{O}$ ;  $\text{C}_6\text{A}\hat{\text{S}}\text{H}_{32}$ ) except for OG30F20, of which the AFt phase was not observed in the curve at the identical condition. As shown in Fig. 2b, especially, there is a distinct difference in the peak intensity for CH among the blended cement pastes. For example, the OG30F20 and OG50 samples have a lower value at the degree within  $17.8\text{--}18.4^\circ$  of  $2\theta$ , at which the main peak for CH is observed, while O100 shows relatively strong intensity at the given degree range. The weakened intensity of peak for CH in the binary and ternary system may be due to the latent hydraulic reaction in the cement matrix. In a highly alkaline environment in the OPC system, in fact, a partial replacement of GGBS particles would provide more C–S–H gel, resulting in depletion of CH in the cement matrix. For the case



of the binary system, however, the lower amount of CH may be attributed to the delayed hydration. The peak intensity for unhydrated cement particles in the paste, in particular for C3S, still remained high, indicating the hydration degree is lower at the given condition. This observation may mean that a lower intensity for CH in OG50 sample is responsible for less hydration. Moreover, available space for hydration products can be provided by substitution of the lower hydraulic binder at an identical *W/B* ratio, increasing the nucleation sites for the hydrates (Lothenbach et al. 2011). According to Huang et al. (2017), Mg-bearing hydrates were not formed in the FNS-mixed pastes until 90 days. In this study, similarly, the formation of Mg/Fe-based phases originating from forsterite and fayalite in FNS, such as magnesium hydroxide (Mg(OH)<sub>2</sub>; MH), was not observed. Therefore, the ternary blended specimen may be favorable to hydration arising from the extra space in the matrix and would in turn form more C–S–H gel at 28 days of curing.

The latent hydration is confirmed by quantitative analysis for content of hydration products, including CH and C–S–H phases, using TG method, which is a technique measuring the mass change of phases during gradually heating under nitrogen atmosphere to avoid carbonation. When the TG curve is differentiated by temperature (i.e., DTG), it is possible to identify the presence of the hydrates. Moreover, the 2nd derivative of the TG curve can produce the temperature range of decomposition for the phases, substantially estimate the quantity of the hydrates using the following equation:

$$\text{Weight of phase} = \text{ML}_{\text{phase}} \times \frac{m_{\text{phase}}}{m_{\text{H}_2\text{O}}}, \tag{4}$$

where  $\text{ML}_{\text{phase}}$  is the mass loss of phase at a given temperature range (%),  $m_{\text{phase}}$  is the molecular mass of phases (g/mol) and  $m_{\text{H}_2\text{O}}$  is the molecular mass of water (g/mol). Figure 3 presents the result of TG–DTG for the blends cured at 28 days, of which mass loss at around 100 and 450 °C indicates decomposition of C–S–H gel and CH. For the O100, the CH content in the paste calculated from the TG–DTG curve is 20.3%, while OG50 and OG30F20 account for 4.9% and 11.5%, respectively. As mentioned above, however, the lower value for the OG50 is presumably due to delayed hydration process, rather than arising from the diminishing of CH in the extended reaction. Simultaneously, the quantity of C–S–H gel in each sample might also support this assumption. The OG30F20 shows the highest value in the content of C–S–H gel accounting for 69.9%, but OG50 indicates 59.4%, which is even lower than the O100 (61.0%). In addition, a similar hydration behavior was confirmed by Lemonis et al. (2015). The authors conducted XRD and TGA test for the cement paste containing FNS and

natural pozzolanic materials with time and concluded that the ternary system could encourage the formation of C–S–H in the matrix after 28 days of curing. Therefore, the partial replacement of GGBS and FNS with OPC would provide a higher activity in the latent hydration.

### 3.2 Fundamental Properties of Blended Concretes

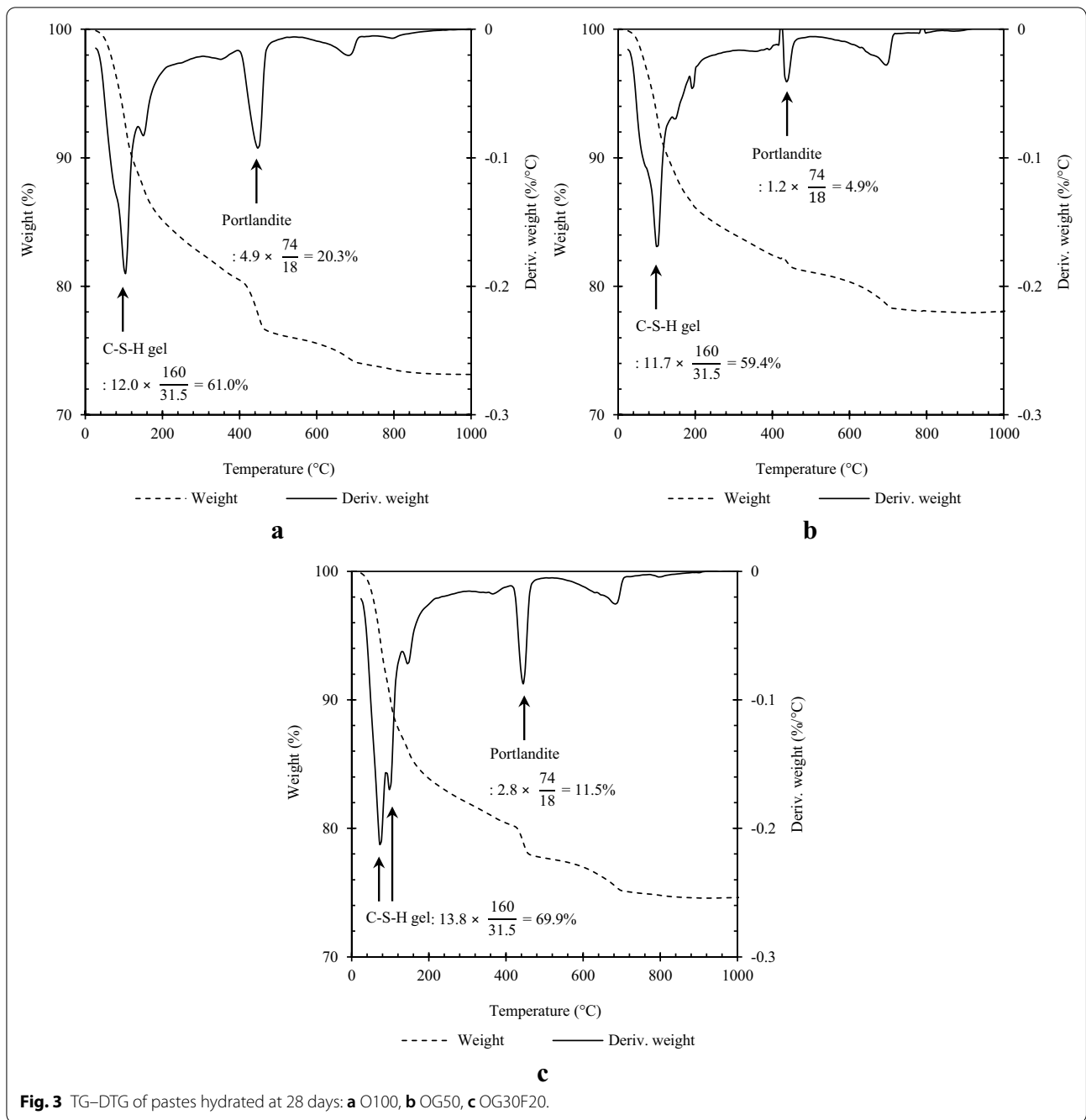
The pore size distribution of concrete with three different mix proportions at 28 days was determined by MIP to investigate the influence of GGBS and FNS substitution on pore structure in the matrix, as given in Fig. 4 and Table 4.

The curves were plotted by the incremental and cumulative intrusion volume with different sizes. The range of pore size was categorized as follows (Mindess et al. 1981):

1. small capillary (<0.01 μm);
2. medium capillary (0.01–0.05 μm);
3. large capillary (0.05–10 μm); and
4. void (> 10 μm).

It is seen that the total intruded volume at 28 days is affected by the binder system; O100 has the highest value accounting for 0.188 mL/g, followed by 0.174 and 0.151 for OG50 and OG30F20, respectively. In addition, it is noticeable that porosity at small capillary for OG30F20 is remarkably higher than that for other mixes. For example, OG30F20 indicates 11.64% for small-capillary porosity, while the value of 1.49 and 2.59% is accounted for O100 and OG50, respectively. This result is consistent with the content of C–S–H gel calculated by TGA results for pastes cured at 28 days. As can be seen in Fig. 3, OG30F20 has the highest content of C–S–H gel, presumably due to latent hydration and/or pozzolanic reaction of GGBS and FNS, thereby modifying the pore structure of the matrix. The formation of C–S–H gel may represent the higher fraction of small capillary pore, which is usually formed within the hydrates. Thus, the volume of inner pores would be increased with time when used GGBS and FNS as the binder. For a more precise investigation of the gel pore in the matrix, however, additional experiments such as helium or nitrogen gas absorption must be conducted.

Development of compressive strength for the concrete made with GGBS and FNS was measured for 180 days, as shown in Fig. 5. It is seen that the OPC concrete has the highest strength at all ages, but strength development depends on the binder system. For example, the early strength (7 days) for O100 is 35.4 MPa, while OG50 and OG30F20 indicate 24.7 and 26.4 MPa, respectively. With increasing time, binary and ternary system show a rapid increase in the strength at 28 days compared to O100, accounting



for 34.0 and 37.8 MPa, whose values are equal to 37.8 and 42.6% of an increased ratio than 7-day strength. In fact, partial substitution of OPC by GGBS produces a lower strength at early ages due to a lower reactivity of the binder (Neville 1995; Matthes et al. 2018). Also, FNS replacement as binder provides a reduced strength within 90 days at normal environments, compared to only OPC mixes (Rahman et al. 2017; Huang et al. 2017). In long-term hydration, however, a gain

in strength would be advanced due to a latent and/or pozzolanic reaction. Moreover, a surplus of space for hydration products arising from the replacement of binders, possessing a lower reactivity, at an identical water content could contribute to hydration degree, thereby increasing the strength. In a previous study (Lemonis et al. 2015), mortar specimens containing GGBS and FNS performed quite higher strength than OPC-GGBS mixed ones until 56 days, but the OPC

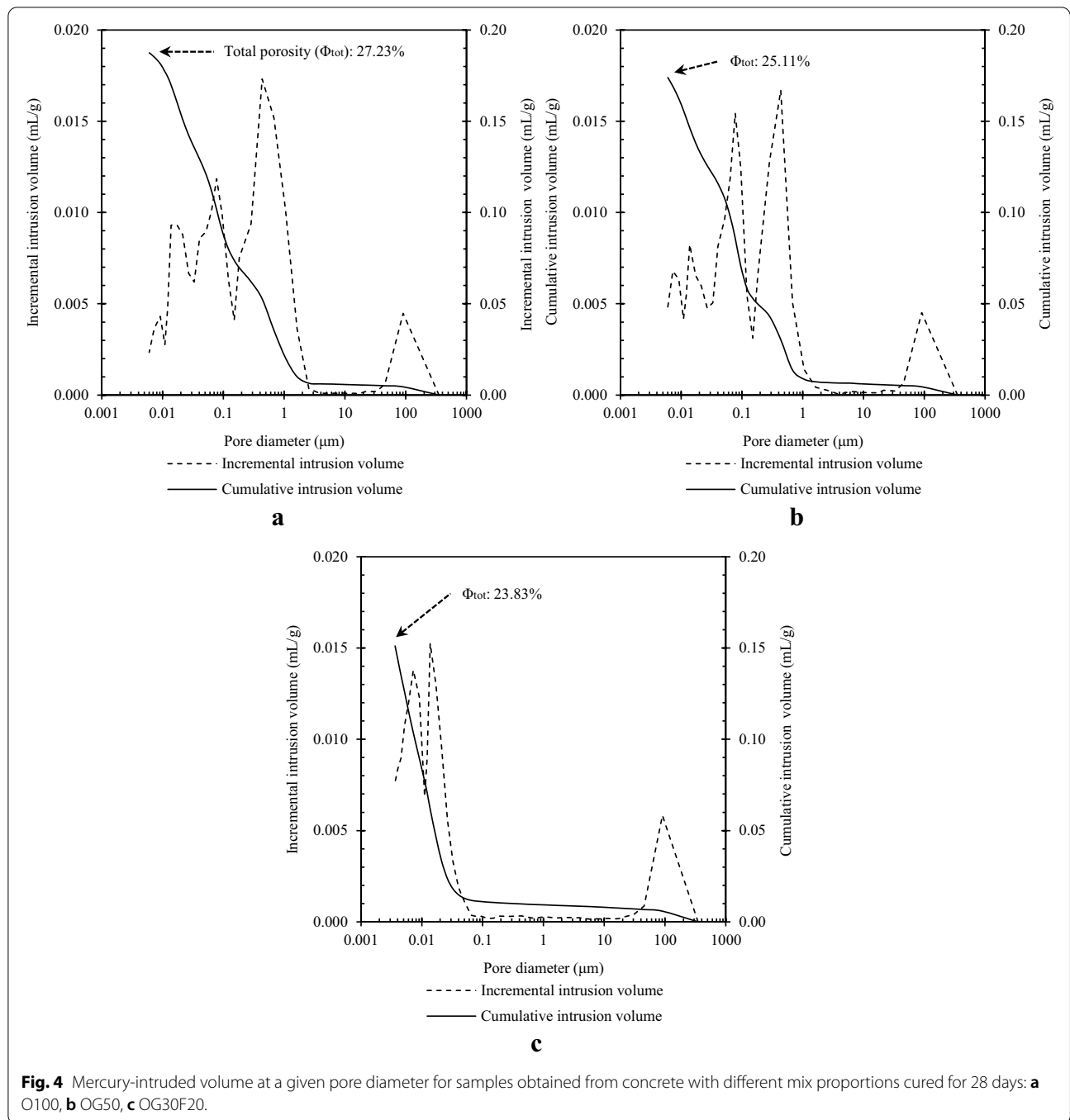
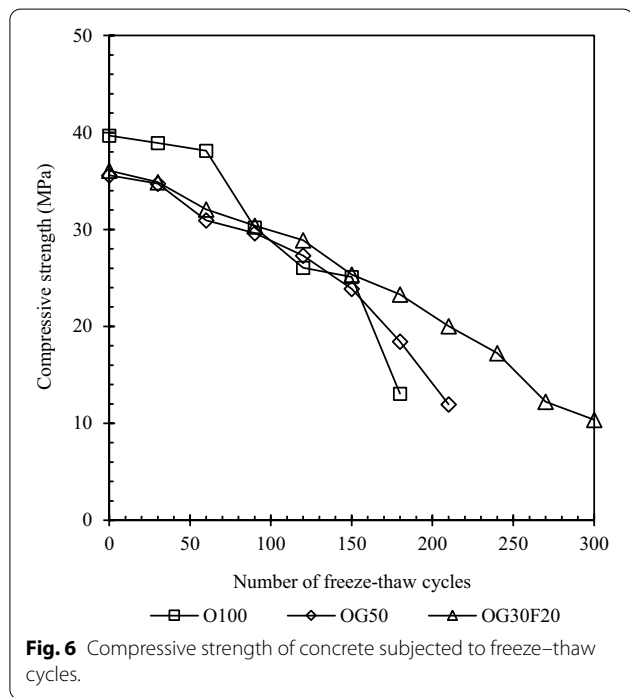
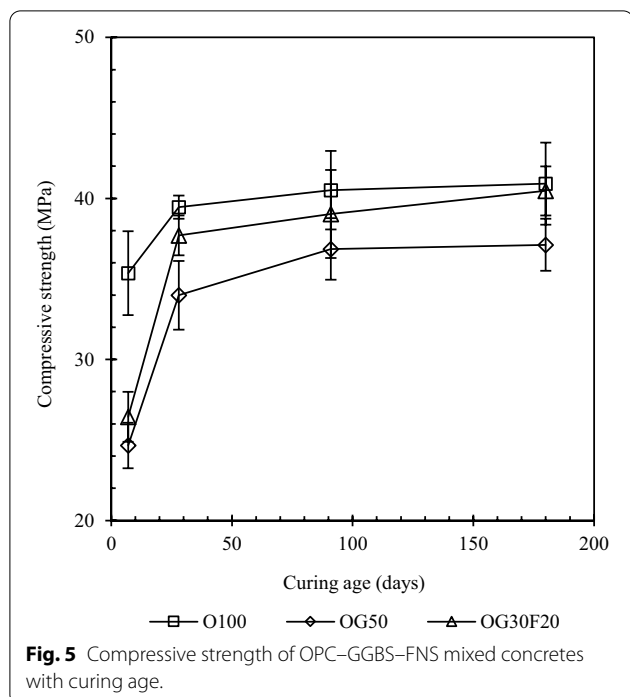


**Fig. 4** Mercury-intruded volume at a given pore diameter for samples obtained from concrete with different mix proportions cured for 28 days: **a** O100, **b** OG50, **c** OG30F20.

**Table 4** Classification of pore sizes in hydrated paste (%).

	O100	OG50	OG30F20
Void	0.85	0.89	1.27
Large capillary	16.71	14.66	0.76
Medium capillary	8.18	6.97	10.17
Small capillary	1.49	2.59	11.64
Total	27.23	25.11	23.83

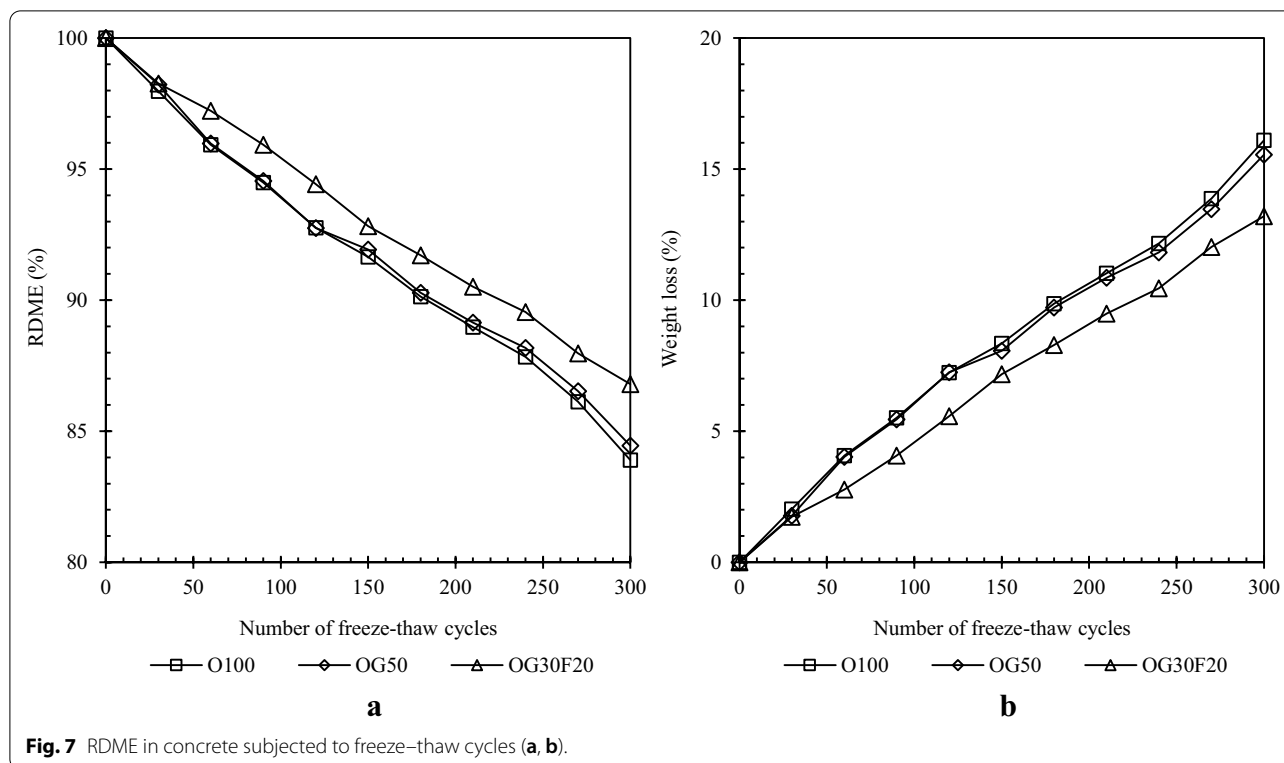
showed the highest value at all ages. This behavior is confirmed in this study that the strength of OG30F20 was always higher than that of OG50. Even after 91 days of curing, the terminal strength for OG30F20 indicates 40.5 MPa, which is close to that for O100. However, there is no distinct relation between pore structure and compressive strength for the concretes at 28 days.



**3.3 Resistance of Blended Concrete to Freeze–Thaw Cycles**  
 During exposure of the concrete specimens to repeated freeze–thaw cycles up to 300 cycles, the compressive strength for three types of concrete specimens was measured at every 30 cycles, as given in Fig. 6. The initial

strength for O100, OG50 and OG30F20 (i.e., 28-day compressive strength) is 39.5, 34.0 and 37.7 MPa, respectively. The compressive strength decreases with the number of cycles, regardless of the binder systems. This may imply that the pore structure in the matrix was presumed to be more porous in the duration of the freeze and thaw environments, due to the internal stress resulting from ice formation in the pore solution of the concrete. This pressure could be, in fact, accumulated continuously within water-filled pores, even when separated from each other. Thus, the concrete matrix can be destroyed in the process of the freeze–thaw cycles, resulting in a decrease in the strength. It is notable that a rate of the reduction in the strength for ternary blended concrete is mitigated compared to other mixes. For example, the measurement for OG30F20 lasts at a given exposure period (300 cycles), while O100 and OG50 show a shorter time to reach an unavailable state for conducting the test, at which the finished term is 180 and 210 cycles, respectively. This is presumably attributed to a lower threshold temperature for the formation of ice in pore solution at a gel realm, in which the water can be frozen at below  $-78\text{ }^{\circ}\text{C}$  (Neville 1995). As described in the previous sections (Figs. 3 and 4), the content of C–S–H gel in the paste consisting of GGBS and FNS (i.e., OG30F20) was higher than that in O100 and OG50. An increase in the smaller pore in the matrix arising from more generation of the C–S–H phase may impose a decrease in the freezing point of the water within the hydrates (Ann et al. 2017; Liu et al. 2018). Then, the deterioration level of the concrete subjected to freeze and thaw cycles would be lowered in the long term.

This phenomenon is also supported by the variation in the RDME and weight loss of the concretes subjected to freeze and thaw cycles, as given in Fig. 7. An increase of the number of cycles results in a decrease in the RDME and simultaneously an increase in the weight loss, irrespective of the binder systems. In the process of freeze–thaw cycles, an increase of the further porosities within the concrete matrix may cause higher connectivity between pores, producing a higher value of frequency of the concrete. After a certain level of degradation due to frost attack, links between the cracking-originated pores in the vicinity of the concrete surface would induce the spalling of cover concrete and subsequently result in a weight loss of the specimen. When the water-filled pore is much smaller to freeze at a given temperature (i.e.,  $-18\text{ }^{\circ}\text{C}$ ), however, the influence of repeated freeze–thaw cycles on the concrete would be less vulnerable. Thus, the concrete with higher porosity at small pore size can be increased to frost damage. In this study, the ternary concrete shows a lower level for the variation of the RDME and weight loss at an identical condition, compared with O100 and OG50. At 300 cycles of repeated freeze and



thaw, for example, O100, OG50 and OG30F20 achieve 83.9, 84.5 and 86.8% for the RDME and simultaneously 16.1, 15.6 and 13.21% for weight loss of the concrete, respectively. Therefore, it can be said that the ternary system with the higher content of C–S–H gel may benefit in enhancing the resistance to the freeze–thaw environment at a given curing regime, even without the use of air entraining agent. However, all specimens used in this study achieved the requirement level to ensure the safety of concrete structures as per the ASTM C 666 guidance (i.e., 60% in the RDME at 300 cycles of freeze and thaw); it may be ascribed to mix design used in this study securing 5–6% of air content for all concretes.

#### 4 Conclusions

In this study, the influence of concrete with different binder systems on resistance to frost damage, of which the cement was replaced by the GGBS and FNS at the given proportions, was investigated by the RDME and weight loss under the repeated freeze–thaw cycles. These results were supported by further experimental works including the development of strength for 180 days of curing, and meanwhile the identification of hydrates in the cement matrix by XRD and DTG and the examination of the pores structure using mercury intrusion porosimetry were conducted at 28 days. The GGBS and FNS were replaced with 50 and 0%, and 30 and 20%

by weight of mass for OG50 and OG30F20, respectively. Details obtained from the present study are as follows:

1. The replacement of the FNS and GGBS with OPC resulted in an increase of C–S–H gel content due to the latent hydraulic and pozzolanic reactions, which is identified from the relative lower intensity of the main peak for CH in the XRD curves for the OG50 and OG30F20. In the process of quantification of phases using the TGA method, moreover, the decrease in CH content with simultaneous increase in the content of C–S–H gel is confirmed when both of FNS and GGBS were used as the binder.
2. A modification of pore structure obviously showed that the substitution of GGBS and FNS resulted in an increase in the intrusion volume of mercury at a given range for small capillary, accounting for 11.64%, which supports the results of the quantitative/qualitative analysis for the phases.
3. Concrete made with only OPC, kept at 0.45 of *W/B*, showed the highest values in the compressive strength at all ages. However, the strength for the ternary binder system was continuously increased with time and eventually reached at the similar level to O100 at 180 days of curing (40.47 MPa), while strength for the binary system was always lower irrespective of the curing ages.

4. When concrete is exposed to cyclic freezing and thawing environment, the compressive strength was decreased by the number of cycles. Particularly for OG30F20, the measurement was continued for 300 cycles, while O100 and OG50 were destroyed at 180 and 210 cycles, respectively. Similarly, the RMDE and weight loss of the ternary system demonstrated the highest resistance to the deterioration due to the higher content of C–S–H gel in the matrix.

#### Authors' contributions

WJC conceived and designed the experiments; WJC performed the experiments; MJK analyzed the data; WJC wrote the paper. All authors read and approved the final manuscript.

#### Authors' information

Won Jung Cho, Ph.D., Department of Civil and Environmental Engineering, Hanyang University, Ansan 15588, Republic of Korea. Min Jae Kim, Research Professor in Department of civil, Environmental and Architecture Engineering, Korea University, Seoul 02841, Republic of Korea.

#### Funding/acknowledgements

This work was supported by the National Research Foundation of Korea [Grant number: 2020R1A2C3012248].

#### Availability of data and materials

All data have been disclosed in this manuscript.

#### Competing interests

The authors declare that they have no competing interests.

#### Author details

<sup>1</sup> Department of Civil and Environmental Engineering, Hanyang University, Ansan 15588, Republic of Korea. <sup>2</sup> Department of Civil, Environmental and Architecture Engineering, Korea University, Seoul 02841, Republic of Korea.

Received: 23 July 2020 Accepted: 12 November 2020

Published online: 21 January 2021

#### References

- Ann, K. Y., Kim, M. J., Hwang, J. P., Cho, C. G., & Kim, K. H. (2017). Chloride transport in OPC concrete subjected to the freeze and thaw damage. *Advances in Materials Science and Engineering*. <https://doi.org/10.1155/2017/8212856>.
- Cho, B. S., Kim, Y. U., Kim, D. B., & Choi, S. J. (2018). Effect of ferronickel slag powder on microhydration heat, flow, compressive strength, and drying shrinkage of mortar. *Advances in Civil Engineering*. <https://doi.org/10.1155/2018>.
- Choi, Y. C., & Choi, S. (2015). Alkali–silica reactivity of cementitious materials using ferro-nickel slag fine aggregates produced in different cooling conditions. *Construction and Building Materials*, *99*, 279–287. <https://doi.org/10.1016/j.conbuildmat.2015.09.039>.
- Ghods, P., Alizadeh, R., & Salehi, M. (2017). *U.S. Patent No. 9,638,652*. Washington, DC: U.S. Patent and Trademark Office.
- Huang, Y., Wang, Q., & Shi, M. (2017). Characteristics and reactivity of ferronickel slag powder. *Construction and Building Materials*, *156*, 773–789. <https://doi.org/10.1016/j.conbuildmat.2017.09.038>.
- JSCE Committee. (1994). Guidelines for construction using Ferronickel slag fine aggregate concrete. *Concr. Libr. JSCE*, *24*. <http://www.jsce.or.jp>.
- Juenger, M. C., & Siddique, R. (2015). Recent advances in understanding the role of supplementary cementitious materials in concrete. *Cement and Concrete Research*, *78*, 71–80. <https://doi.org/10.1016/j.cemconres.2015.03.018>.
- Katsiotis, N. S., Tsakiridis, P. E., Velissariou, D., Katsiotis, M. S., Alhassan, S. M., & Beazi, M. (2015). Utilization of ferronickel slag as additive in Portland cement: A hydration leaching study. *Waste and Biomass Valorization*, *6*(2), 177–189. <https://doi.org/10.1007/s12649-015-9346-7>.
- Koh, K. T., & Ryu, G. S. (2011). Strength development and freeze–thaw concrete incorporating high volume blast-furnace slag subjected to initial frost damage. *Journal of the Korea Recycled Construction Resources Institute*, *15*, 79–87.
- KS L 5106. (2009). *Testing method for fineness of Portland cement by air permeability apparatus, Korean Industrial Standards*.
- Lemonis, N., Tsakiridis, P. E., Katsiotis, N. S., Antiohos, S., Papageorgiou, D., Katsiotis, M. S., & Beazi-Katsioti, M. (2015). Hydration study of ternary blended cements containing ferronickel slag and natural pozzolan. *Construction and Building Materials*, *81*, 130–139. <https://doi.org/10.1016/j.conbuildmat.2015.02.046>.
- Liu, L., Wang, X., Zhou, J., Chu, H., Shen, D., Chen, H., & Qin, S. (2018). Investigation of pore structure and mechanical property of cement paste subjected to the coupled action of freezing/thawing and calcium leaching. *Cement and Concrete Research*, *109*, 133–146. <https://doi.org/10.1016/j.cemconres.2018.04.015>.
- Lothenbach, B., Scrivener, K., & Hooton, R. D. (2011). Supplementary cementitious materials. *Cement and Concrete Research*, *41*(12), 1244–1256. <https://doi.org/10.1016/j.cemconres.2010.12.001>.
- Mahasen, N., Smith, S., & Humphreys, K. (2003). The cement industry and global climate change: current and potential future cement industry CO<sub>2</sub> emissions. In *Greenhouse gas control technologies-6th international conference* (pp. 995–1000). Pergamon.
- Matthes, W., et al. (2018). Ground granulated blast-furnace slag. *Properties of fresh and hardened concrete containing supplementary cementitious materials* (pp. 1–53). Cham: Springer.
- Mindess, S., Young, J. F., & Darwin, D. (1981). *Concrete* (p. 481). Englewood Cliffs, NJ: Prentice-Hall.
- Neville, A. M. (1995). *Properties of concrete* (Vol. 4). London: Longman.
- Öner, M., Erdoğdu, K., & Günlü, A. (2003). Effect of components fineness on strength of blast furnace slag cement. *Cement and Concrete Research*, *33*(4), 463–469. [https://doi.org/10.1016/S0008-8846\(02\)00713-5](https://doi.org/10.1016/S0008-8846(02)00713-5).
- Pang, L., Ma, Z., & Xie, Y. (2015). Preliminary study on the preparation of self-compacting concrete used by ferronickel slag micro powder. In *Proceedings of the 1st conference on solid waste utilization and eco-materials, China, Beijing* (pp. 68–72) (in Chinese with English abstract).
- Rahman, M. A., Sarker, P. K., Shaikh, F. U. A., & Saha, A. K. (2017). Soundness and compressive strength of Portland cement blended with ground granulated ferronickel slag. *Construction and Building Materials*, *140*, 194–202. <https://doi.org/10.1016/j.conbuildmat.2017.02.023>.
- Saha, A. K., & Sarker, P. K. (2016). Expansion due to alkali–silica reaction of ferronickel slag fine aggregate in OPC and blended cement mortars. *Construction and Building Materials*, *123*, 135–142. <https://doi.org/10.1016/j.conbuildmat.2016.06.144>.
- Saha, A., & Sarker, P. (2017). Compressive strength of mortar containing ferronickel slag as replacement of natural sand. *Procedia Engineering*, *171*, 689–694.
- Saha, A. K., & Sarker, P. K. (2018a). Durability of mortar incorporating ferronickel slag aggregate and supplementary cementitious materials subjected to wet–dry cycles. *International Journal of Concrete Structures and Materials*, *12*(1), 1–12. <https://doi.org/10.1186/s40069-018-0237-8>.
- Saha, A. K., & Sarker, P. K. (2018b). Durability characteristics of concrete using ferronickel slag fine aggregate and fly ash. *Magazine of Concrete Research*, *70*(17), 865–874. <https://doi.org/10.1680/jmacr.17.00260>.
- Sakoi, Y., Aba, M., Tsukinaga, Y., & Nagataki, S. (2013). Properties of concrete used in ferronickel slag aggregate. In *Proceedings of the 3rd international conference on sustainable construction materials and technologies, Tokyo, Japan* (pp. 1–6).
- Scrivener, K. (2012). Issues in sustainability in cements and concrete. *American Ceramic Society Bulletin*, *91*, 47–50.
- Winter, N. B. (2012). *Understanding cement: An introduction to cement production, cement hydration and deleterious processes in concrete*. Saint Ives: Microanalysis Consultants.

#### Publisher's Note

Springer Nature remains neutral with regard to jurisdictional claims in published maps and institutional affiliations.